

GHz Operation of Nanometer-Scale Metallic Memristors: Highly Transparent Conductance Channels in Ag_2S Devices

A. Geresdi, M. Csontos,* A. Gubicza, A. Halbritter, and G. Mihály

Department of Physics, Budapest University of Technology and Economics and
Condensed Matter Research Group of the Hungarian Academy of Sciences, 1111 Budapest, Budapest ut 8, Hungary

(Dated: September 15, 2021)

The nonlinear transport properties of nanometer-scale junctions formed between an inert metallic tip and an Ag film covered by a thin Ag_2S layer are investigated. Suitably prepared samples exhibit memristive behavior with technologically optimal ON and OFF state resistances yielding to resistive switching on the nanosecond time scale. Utilizing point contact Andreev reflection spectroscopy we studied the nature of electron transport in the active volume of the memristive junctions showing that both the ON and OFF states correspond to truly nanometer scale, highly transparent metallic channels. Our results demonstrate the merits of Ag_2S nanojunctions as nanometer-scale memory cells with GHz operation frequencies.

The ongoing miniaturization beyond the limitations of nowadays CMOS technology is a major challenge in nanosciences [1–3]. Using individual atoms or molecules in nanoelectronic circuits has been a breakthrough towards the ultimate single atomic size limit [4, 5]. The persisting technological difficulties in the reliable assembly of low resistance single molecule devices, however, still represent a major barrier to fast applications preferring low RC time constants with the capacitance of the environment. Alternatively, reversible solid state electrochemical reactions have been proposed to form tunable atomic scale junctions between metallic electrodes. The first results are extremely promising for the short term realization of highly integrated information storage applications [6–13]. The resistive state of such a memory element, called *memristor* [6, 8, 9, 14–16], is altered by biasing the device above its writing threshold V_{th} . Readout is performed at lower signal levels which preserve the stored information.

Chalcogenide compounds have been put forward in the context of the “atomic switch” [7], consisting of an inert metallic electrode (Me) and a Ag layer capped with the solid state ionic conductor Ag_2S . Upon positively biasing the Ag electrode with respect to Me, a metallic Ag propulsion is grown on the Ag_2S -Me interface shunting the electrodes thus creating the non-volatile ON state of the device [17–21]. Real-time high resolution transmission electron microscopy (HRTEM) imaging [22] and first principle band structure calculations [23, 24] suggested that a structural phase transition in the Ag_2S layer also plays a role in the resistive transition [25].

Since the pioneering experiments reported on Ag- Ag_2S -Pt devices [7] the development of memory cells based on memristive systems has achieved a remarkable progress. Beside providing an interesting model system for neural networks [26–28] Ag_2S based devices have been utilized as nanometer-scale non-volatile memory elements [7, 21]. However, the best performing Ag_2S devices [7] have been operated only up to ~ 10 MHz frequencies presumably due to the typically ≥ 100 $\text{k}\Omega$ OFF

state resistances which require the monitoring of technically unfavorable low currents and give rise to larger RC time constants which are inconvenient for GHz applications [29]. In a tantalum oxide based system sub-nanosecond switching times were shown [13] in a significantly larger, lithographically defined structure whose operation relies on the reconfiguration of oxygen vacancies. Here we demonstrate devices which not only approach the atomic size limit but are also capable of GHz operation.

We study resistive switching in voltage biased nanojunctions created between inert metallic tips and 10–100 nm thick Ag_2S surface layers deposited on Ag thin film samples by using an STM setup as illustrated schematically in the inset of Fig. 1(a). While longer sulfur deposition times resulted in semiconducting Ag_2S layers in agreement with previous reports [18–20], below an approximate thickness of 20 nm metallic conductance with technologically optimal device resistances was found over the wide temperature range of 4.2–300 K [30] *both* in the ON and OFF states. These characteristics enable GHz operation. Here we focus on switching phenomena observed in such all-metallic junctions. We use a superconducting Nb tip to study the nonlinear differential conductance on the voltage scale of the superconducting gap, $eV \leq \Delta = 1.4$ meV $\ll V_{\text{th}}$. By utilizing the theory of charge conversion at the interface of a normal metal and a superconductor [31–34] we quantitatively evaluate the reconfiguration of the conducting channels in the nanojunction and thus demonstrate that resistive switching takes place in highly transparent devices with an effective junction area of 2–5 nm in diameter.

Numerous nanoscale contacts with reproducible I-V characteristics were created by gently touching the sample surface with a mechanically sharpened PtIr or Nb tip. The ON and OFF state resistances R_{ON} and R_{OFF} were probed in a narrow voltage window of ± 50 mV $\ll V_{\text{th}}$. For more experimental details see the Appendix and Refs. 30, 35.

A typical room temperature I-V trace is shown in

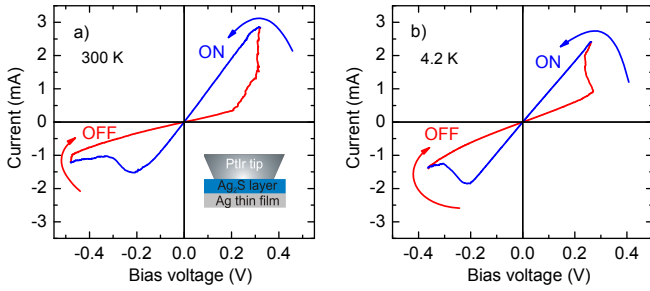


FIG. 1. (Color online) Typical I-V characteristics of Ag_2S based memristive junctions at room temperature (a) and at 4.2 K (b). Positive voltage corresponds to the positive biasing of the Ag layer with respect to the PtIr electrode. The arrows indicate the direction of the bias sweep. The inset shows the schematic cross section of the sample.

Fig. 1(a) for a PtIr tip. Applying an increasing positive voltage on the Ag electrode in the high resistance ($R_{\text{OFF}} \approx 0.5 \text{ k}\Omega$) state first a linear current-voltage dependence is observed. At $V_{\text{th}} \approx 300 \text{ mV}$ the junction switches to its low resistance ON state ($R_{\text{ON}} \approx 0.1 \text{ k}\Omega$). At a subsequent decrease of the bias a linear dependence is observed until the negative threshold voltage is reached where the OFF state is restored. The slight backward turning of the onset of the OFF to ON switching arises due to the compensation for the finite, 50–200 Ω serial resistance of the voltage biasing circuit. By limiting the current in the ON state, this serial resistance also plays a role in maintaining the stability of the junctions. The observed switching scheme is ideal for memory applications, as the device can be switched between the two states at a reasonably high bias while R_{ON} and R_{OFF} are optimal for fast readout at low bias.

A similar I-V trace is obtained at 4.2 K as shown in Fig. 1(b) testifying to the metallic nature of the system. The linear ON and OFF traces and the wide range of operation temperature contradict to the thermally activated ionic migration in bulk Ag_2S [29]. The observed metallic behavior is consistent with first principle calculations applicable to a thin surface layer of Ag_2S deposited on bulk Ag which is expected to undergo a structural phase transition called spontaneous metallization [23]. Next we investigate this metallized state experimentally by replacing the PtIr tip by superconducting Nb and utilizing point contact Andreev reflection (PCAR) spectroscopy [31–34].

This method is inspired by the fact that linear conductance measurements alone cannot distinguish between fundamentally different types of junctions exhibiting the same conductance. The conductance of a nano-scale device is given as $G = 2e^2/h \cdot M \cdot T$, where T is the average electron transmission probability across the device and M is the number of open conductance channels [36, 37]. The latter is approximated as $M \approx (\pi d/2\lambda_F)^2$, where d is the device diameter and λ_F is the Fermi wavelength

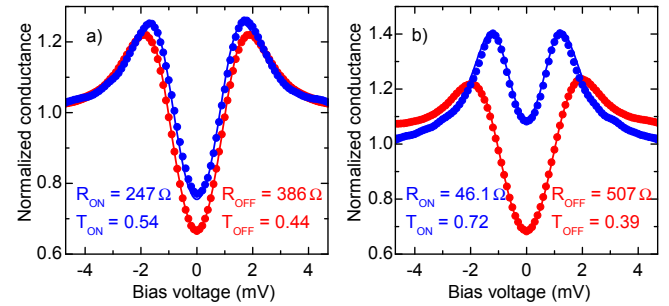


FIG. 2. (Color online) ON and OFF state finite bias differential conductances obtained from the measured I-V traces by numerical differentiation with respect to the bias voltage in two representative $\text{Ag}-\text{Ag}_2\text{S}-\text{Nb}$ junctions at 4.2 K. Each curve is normalized to its high bias ($eV \gg \Delta$) value $G_{\text{ON},\text{OFF}} = (R_{\text{ON},\text{OFF}})^{-1}$. Continuous lines are fits against the BTK theory resulting in the indicated transmissions.

which is $\approx 0.4 \text{ nm}$ in bulk Ag. This simplified picture shows that a $\text{k}\Omega$ range device resistance may as well correspond to a large area tunnel junction ($d \gg \lambda_F$) with very small transmission probability ($T \ll 1$) or, alternatively, to a truly nanometer-scale junction with only a few well transmitting ($T \approx 1$) conductance channels. PCAR measurements performed on the voltage scale of Δ can distinguish between these extremities via the non-linear transport properties of a point contact connecting a normal metal (N) and a superconductor (S) [31]. The transmission can be evaluated by fitting the voltage dependent differential conductance with the model of Blonder, Tinkham and Klapwijk (BTK) [32, 33].

Figure 2 shows the finite bias differential conductance of the ON and OFF states in two representative junctions exhibiting a minor [Fig. 2(a)] and an order of magnitude [Fig. 2(b)] change in the normal-state differential conductance G_N upon switching. The typical switching threshold voltages of $V_{\text{th}} \approx 300\text{--}800 \text{ mV}$ are well separated from the N-S features taking place at the voltage scale of Δ . The effective transmissions were determined by fitting the differential conductance curves against the modified version of the BTK theory, incorporating a Γ broadening parameter which is necessary to account also for contact diameters comparable to the electronic mean free path [38, 39]. With this extension the spin degenerate model contains five parameters: the temperature, Δ , G_N , Γ and T . A numerically reliable and physically meaningful fitting procedure, however, requires the reduction of such an extended parameter space to a minimum set of key parameters. After taking extra care of the proper thermal anchoring of the device leads in our ${}^4\text{He}$ cryostat we fixed the temperature value to 4.2 K. Finite bias tunneling measurements ($R_{\text{contact}} > 100 \text{ k}\Omega$) carried out on $\text{Ag}-\text{Ag}_2\text{S}-\text{Nb}$ samples and on clean Au foils revealed that the bulk value of $\Delta = 1.4 \text{ meV}$ is a good approximation also in our point contact arrangement. In these data, Γ

stayed below 5% of Δ quantifying the voltage noise of our setup. After evaluating G_N from the high bias linear slopes of the raw I-V traces, the BTK fittings were run with two free parameters T and Γ .

In device 1 [Fig. 2(a)] $R_{\text{ON}} = 247 \Omega$ and $R_{\text{OFF}} = 386 \Omega$, the corresponding transmission probabilities are 0.54 and 0.44, whereas the effective numbers of open conductance channels, estimated as $M = G_N/G_0T$, are 118 and 62, respectively. This shows that both the ON and OFF states are characterized by rather large transmission values and the 56% change of the conductance between the two states is equally attributed to the variations in M and T . In device 2 [Fig. 2(b)] the order of magnitude change in G_N ($G_{\text{ON}}/G_{\text{OFF}} = 11$) is accompanied by a large change in M ($M_{\text{ON}}/M_{\text{OFF}} = 6.2$) and a minor change in T ($T_{\text{ON}}/T_{\text{OFF}} = 1.8$). The ON and OFF state effective contact diameters are estimated to be $d_{\text{ON}} = 2.7 \text{ nm}$ and $d_{\text{OFF}} = 2 \text{ nm}$ in device 1 and $d_{\text{ON}} = 5 \text{ nm}$ and $d_{\text{OFF}} = 2.1 \text{ nm}$ in device 2, demonstrating that resistive switching takes place in truly nanometer-scale junctions.

In order to verify the statistical relevance of these findings, T and d were evaluated for various junctions yielding to $T_{\text{ON}} = 0.62 \pm 0.1$ and $T_{\text{OFF}} = 0.42 \pm 0.07$ at effective junction diameters of $d = 2\text{--}5 \text{ nm}$. Figure 3 shows the relative changes in T and M upon switching as a function of the resistance ratio of the corresponding ON and OFF states. The two limiting cases of the unchanged transmissions and unchanged channel numbers are indicated in Figs. 3(a) and 3(b) by the orange and green dash lines and are also schematically illustrated in Figs. 3(c) and 3(d), respectively. The numerical accuracy of T is 20% in the OFF states and better than 5% in the ON states as explained in the Appendix and indicated by the error bars in Figs. 3(a) and 3(b). In the studied junctions with ON and OFF state resistances of 50–1000 Ω , Γ is ranging 50–15% of Δ , respectively. These values are significantly higher than those obtained in the tunneling regime in agreement with previous studies carried out on various diffusive systems [39] indicating that in spite of the small junction diameters electron transport is not entirely ballistic due to the rather short mean free path of 1.8 nm in Ag_2S [40].

Our analysis shows that (i) regardless of the relative change in their resistances, all devices exhibit high transmission probabilities in both states corresponding to metallic conductances and (ii) their conductance changes can rather be attributed to a variation in M while T is less significantly changed during the switching. These results give clear evidence that the metallic channels are not completely destructed when the device is switched off, only their effective cross section is reduced while the highly transmitting nature is preserved. This is in good agreement with the presence of spontaneously metallized Ag_2S channels [23] and is in contrast with the simplified picture of the formation and complete destruction of pure Ag nanofilaments. The above characteristics make

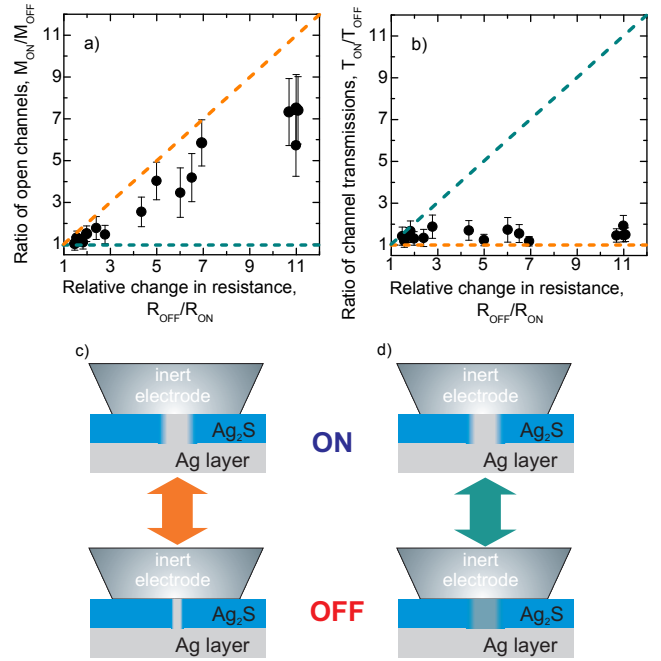


FIG. 3. (Color online) Analysis of the finite bias differential conductance data obtained in various Ag-Ag₂S-Nb devices. The ratios of the number of conducting channels (a) and the average transmission probabilities (b) in the ON and OFF states of each junction are shown as a function of the corresponding relative change in the normal resistance of the devices. The orange dash line displays the limiting case where only M changes as illustrated in (c). The green dash line indicates the opposite scenario when the change in the resistance is solely attributed to the variation of T as illustrated in (d). In the lower panels the width and opacity of the grey region across the Ag₂S layer (blue) represent the number and transmission of the conducting channels, respectively.

Ag₂S based devices particularly suitable to build resistive memory elements with technologically ideal resistances of $\leq 1 \text{ k}\Omega$ and diameters well below the resolution of nowadays lithographic techniques. Note that tunnel junctions of similar sizes would yield to orders of magnitude larger resistances challenging their fast electronic applications.

Finally we demonstrate that the resistive switching of the investigated nanometer-scale metallic channels is a fast process taking place on a nanosecond time scale. Real-time pulsed measurements were performed in vacuum conditions at room temperature by connecting the Ag-Ag₂S-PtIr junction to an arbitrary waveform generator and a digital oscilloscope of 2 ns time resolution via a transmission line in a circuit schematically illustrated in the inset of Fig. 4(b). Subsequent switchings between the ON and OFF states were achieved by voltage pulses of 10 ns duration, 1.5 V amplitude and alternating sign. Between the pulses the device resistance was monitored by applying a 350 mV dc bias. The blue line in Fig. 4(a) shows the applied pulse train in an open circuit configuration when the sample is not connected and the trans-

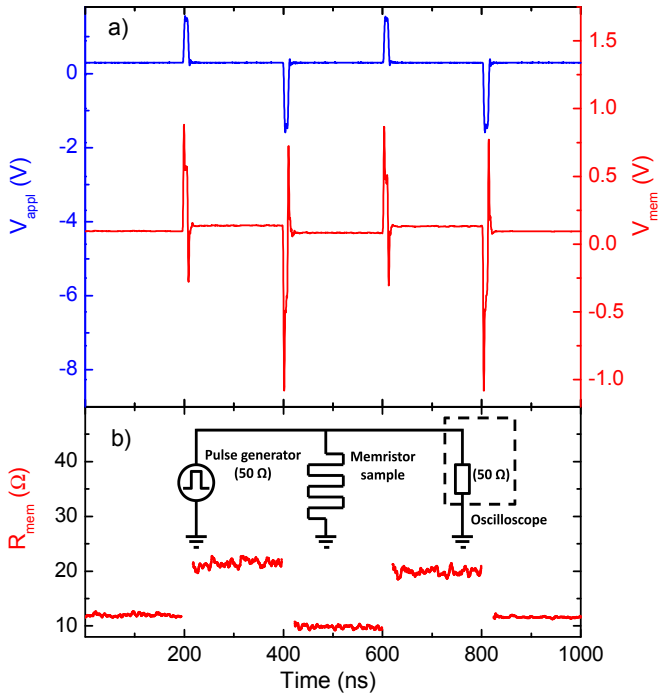


FIG. 4. (Color online) (a) Alternating 10 ns wide voltage pulses (V_{appl} , blue line) recorded in an open circuit configuration and measured on a Ag-Ag₂S-PtIr junction (V_{mem} , red line) at room temperature. During the 200 ns time between the pulses a 350 mV dc read-out voltage was applied. (b) The calculated resistance demonstrates reproducible switching behavior. Data acquired within the pulse duration is not shown. The inset illustrates the equivalent circuit of the setup.

mission line is terminated by an open end resulting in the total reflection of the pulses. In comparison, the red line corresponds to the situation when the transmitted signal from the pulse generator to the scope is superimposed on a partially reflected signal emerging due to the finite resistance of the memristor device. Figure 4(b) shows the calculated resistances of $R_{\text{OFF}}=20 \Omega$ and $R_{\text{ON}}=12 \Omega$. The subsequent, reproducible resistance plateaus are well separated both from each other and from the noise floor of the measurement, satisfying the two most profound requirements of memory applications. While fast pulsing measurements favor contact impedances close to 50 Ω, fast switching at higher contact resistances were also observed, though with lower resolution.

While the ≥ 1.5 ns rise/fall times of our arbitrary waveform generator limit the investigation of shorter time domains by voltage pulses of alternating sign, the single shot experiment shown in Fig. 5 demonstrates that resistive switching in Ag₂S can also be induced by voltage pulses as short as 500 ps. Such measurements were carried out by using a custom built rise time avalanche pulse generator specified to provide unipolar voltage pulses of 500 ps width and ≤ 10 V amplitude [41]. The low bias readout between the short pulses and the subsequent re-

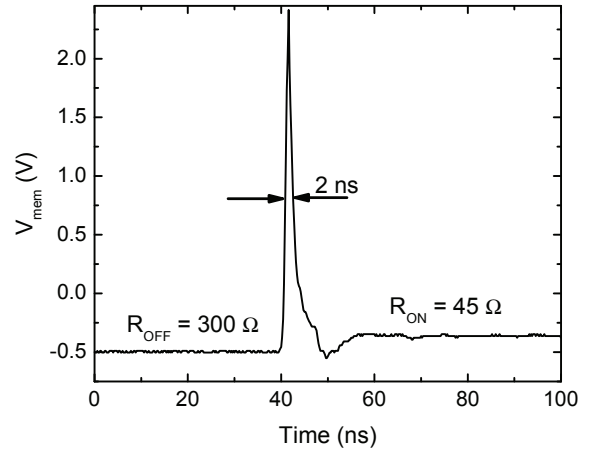


FIG. 5. OFF to ON switching due to a single voltage pulse of 500 ps width and 2.5 V amplitude. The calculated resistance values are indicated. The apparent 2 ns pulse width arises due to the limited detector bandwidth.

initialization of the OFF state were performed by a variable dc offset added to the biasing circuit as explained in the Appendix. Whereas the real-time response of the device is not fully resolved in the experiment due to instrumental and circuit limitations, it is evident that a sub-nanosecond pulse can initiate a resistive switching.

In conclusion, we studied the resistive switching of Ag-Ag₂S-Me memristive nanojunction devices. We showed that by suitable sample preparation reproducible resistive switching and readout can be performed where *both* the ON and OFF states are metallic, characterized by technologically optimal ≤ 1 kΩ resistances and similar device functionalities down to cryogenic temperatures. We introduced PCAR spectroscopy to determine the size and transmission probabilities of the active volume of the devices which revealed a small number of highly transmitting nanoscale conducting channels with reduced but not completely dissolved junction area also in the OFF state. The relatively low resistance ON and OFF states enable fast operation at room temperature as demonstrated by the nanosecond switching times. Our results suggest that Ag₂S represents a promising material basis for a future generation of high speed resistive switching memory devices overriding the downscaling limitations of nowadays CMOS technology.

Enlightening discussions with Ádám Szüllő and his circuit designing contribution to the fast pulsing experiments are acknowledged. This work has been supported by the Hungarian research funds OTKA CNK80991, K105735, TÁMOP 4.2.1.B-09/1-2010-0002. M.C. is a grantee of the Bolyai János Research Scholarship of the HAS and acknowledges financial support of the European Union 7th Framework Programme (Grant No. 293797).

APPENDIX

Ag thin films with a nominal thickness of 80 nm were vacuum evaporated onto a Si substrate. The thin Ag₂S layers were grown by depositing sulfur onto the Ag surfaces in a clean environment. First, analytic grade sulfur powder was loaded in a quartz tube, melted and cooled back in order to ensure a homogenous source. The thin film sample was then loaded in the tube to a distance of 2 cm from the sulfur. After loading both the sulfur and the sample, the tube was evacuated to 10^{-5} mbar pressure. Then the temperature was ramped up to 60 °C and the sublimation of the sulfur was performed in a static vacuum for 2–10 minutes. Finally, the temperature was rapidly ramped down.

The samples were characterized by He-RBS (Rutherford Backscattering Spectrometry) and ERDA (Elastic Recoil Detection Analysis) [35]. They exhibit inhomogeneous sulfur concentration profiles consistent with the presence of an Ag₂S surface layer [30].

Nanoscale contacts were created by gently touching the sample surface with a mechanically sharpened PtIr or Nb tip. For coarse adjustment a screw thread mechanism was used, whereas for the fine positioning a three dimensional piezo scanner was applied. Using this tech-

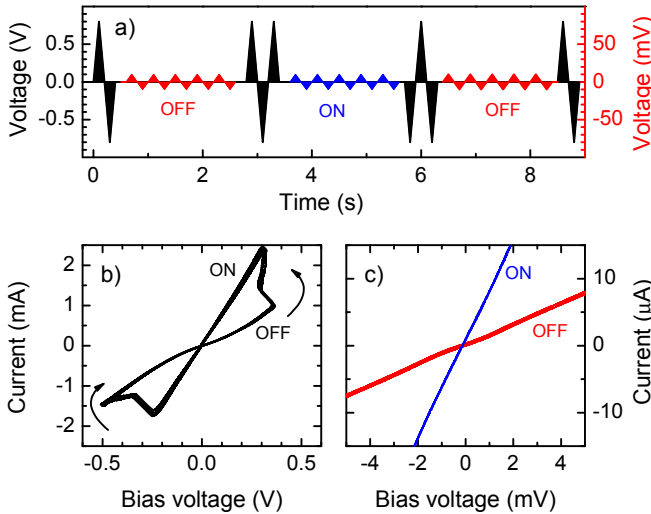


FIG. A1. (a) Biasing scheme of the I-V measurements. The 800 mV amplitude voltage sweeps (black triangles) are used to record the hysteretic switching characteristics and to prepare the subsequent OFF/ON/OFF states for the voltage sweeps performed repeatedly on the scale of the Nb superconducting gap between ± 10 mV (red and blue triangles). (b) Hysteretic high bias I-V characteristics of an Ag-Ag₂S sample and a superconducting Nb tip. The overlap of the 4 subsequent loops demonstrate reproducible resistive switching over the entire pulsing sequence. The arrows indicate the direction of the bias sweep. (c) Low bias I-V traces corresponding to the ON (1 trace) and OFF states (2 overlapping traces). All data were taken at 4.2 K.

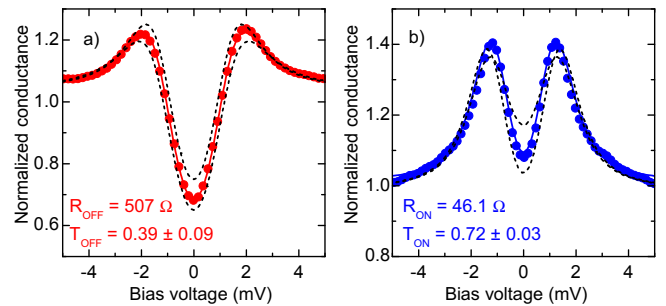


FIG. A2. Representative finite bias conductance in the OFF (a) and ON states (b) of an Ag-Ag₂S-Nb junction at 4.2 K obtained by numerical differentiation of the measured low bias I-V traces. Continuous lines denote fits using the BTK theory with the obtained transmission values shown in the graphs. Note that each curve is normalized to its high bias ($eV \gg \Delta = 1.4$ meV) value $G_{ON,OFF} = (R_{ON,OFF})^{-1}$. The dashed lines correspond to the best fits using the detuned transmission values as labeled in the graphs testifying to the accuracy of our analysis on T .

nique numerous contacts were created with reproducible I-V characteristics. The bias voltage was applied to the junctions by utilizing the analog outputs of a National Instruments data acquisition card. The output voltage was divided and filtered in order to ensure low noise on the contact. The current was measured using a variable range I-V converter and processed by the data acquisition card. The current-voltage characteristics of the junctions were recorded during repeated bias voltage sweeps.

The bias scheme of the I-V measurements carried out with a superconducting Nb tip at 4.2 K is shown in Fig. A1(a). The subsequent resistive switchings are obtained by voltage sweeps of 800 mV amplitude and alternating sign while the ON and OFF state resistances as well as the non-linear current contributions induced by the superconducting tip are detected by low amplitude (± 10 mV) triangular voltage pulses. The first high bias sweep is performed in order to verify the switching and to initialize the device in its OFF state. This is followed by the acquisition of the low bias IV data repeated 5 times for averaging purposes in order to further improve the signal to noise ratio. The next high bias sweep covers one and a half of the total hysteresis loop preparing the device in its ON state before the second sequence of the low bias measurements probing the ON state transport properties are executed. In order to confirm that upon the first OFF to ON switching and ON state measurements the device preserved its reversible configuration, we restored and tested the OFF state again by applying another high bias loop and a low bias sequence, respectively. The reproducibility of the hysteretic high bias I-V traces shown in Fig. A1(b) demonstrate that the two dominant device configurations determining the ON and OFF states did not change over the above sweeping sequences. Fitting the numerical derivative of the low bias

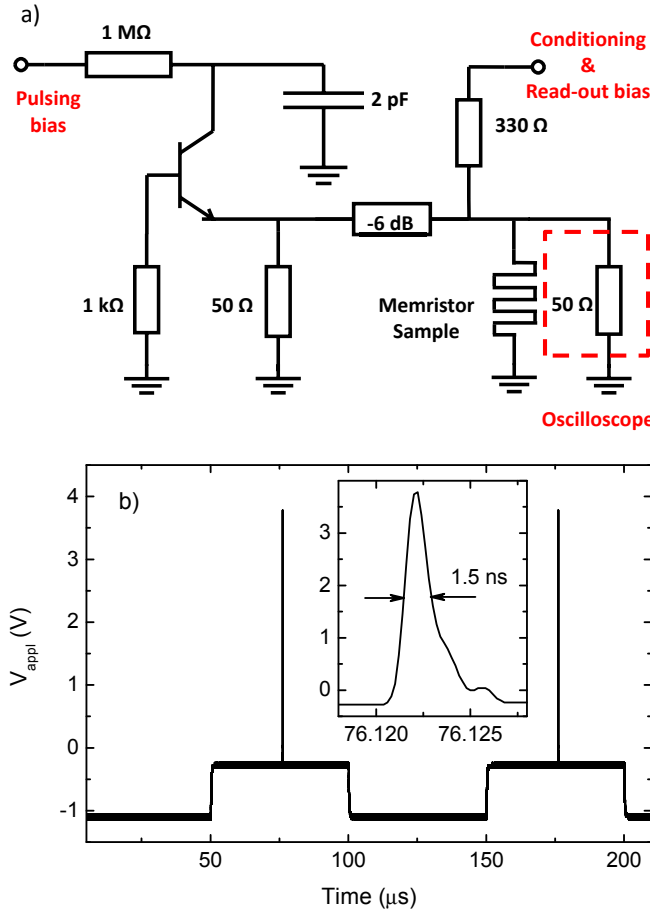


FIG. A3. (a) The circuit layout of the room temperature setup utilized to apply a high (low) negative conditioning (read-out) bias and short voltage pulses of 500 ps duration on the memristor sample. (b) The applied pulsing sequence as recorded in an open circuit configuration. The sample is initialized in its OFF state by the application of the 50 μ s long conditioning pulses of -1.1 V amplitude while the 50 μ s long read-out pulses of -300 mV amplitude are used to determine the status of the device before and after the short pulses. The apparent 1.5 ns width of the nominally 500 ps pulses (inset) is the consequence of the limited, 250 MHz oscilloscope bandwidth.

I-V data displayed in Fig. A1(c) against the BTK theory provides information about the effective transmission values of the corresponding configurations.

The numerical accuracy of the fitting procedure on T is illustrated in Fig. A2. After obtaining the best fitting transmission values by a numerical least square method, T was detuned from its optimum to the values indicated in Fig. A2. The fitting procedure was repeated with the broadening parameter Γ and the superconducting gap Δ as the remaining free parameters while the temperature and the normal state conductance were kept at their predetermined values. The best fitting curves obtained by this procedure are displayed by dashed lines in Fig. A2. Their systematic deviation from the experimental data

demonstrates that the nominated $\Delta T_{\text{OFF}}/T_{\text{OFF}} = 0.20$ and $\Delta T_{\text{ON}}/T_{\text{ON}} = 0.05$ relative errors indeed represent a lower limit on the accuracy of the transmission values determined by the modified BTK model. While the former seems to be a rather conservative estimate, the metallic nature of the OFF states is still evident. Consequently, our attempts to fit the individual differential conductance traces by the parallel contributions of a small, highly transparent channel and a poorly transmitting but extended area junction, the latter dominating G_N , have systematically failed.

The pulsing scheme along with the circuit layout utilized in the room temperature sub-nanosecond pulsing experiments is shown in Fig. A3. The setup is based on a custom built rise time avalanche pulse generator relying on the periodic charging (break-down) of the bipolar transistor indicated in Fig. A3(a) through a 1 MΩ resistor and a 2 pF capacitor (50 Ω resistor) yielding to unipolar outbursts specified to a 500 ps pulse width and ~ 10 V amplitude at a repetition rate of ~ 500 kHz [41]. In order to study the resistive switching behavior of our memristor samples in this unipolar pulsing configuration, the device has to be re-initialized in its OFF state in each cycle of the pulsing sequence by applying a sufficiently large negative bias. The read-out is performed at low negative bias levels applied before and after the short pulses. These slow, typically 50 μ s long signals are added to the biasing circuit via the dc terminal shown in the right hand side of the layout in Fig. A3(a). In order to gain control on the timing of the 500 ps pulses, the onset of the read-out signal is used to gate the 75 V dc bias of the pulse generator. The voltage drop on the memristor sample is monitored by a digital oscilloscope with an effective time resolution of 2 ns. The pulsing sequence shown in Fig. A3(b) was recorded in an open circuit configuration, i.e. when the memristor device is replaced by an open terminal, exhibiting transient behavior decaying within 3 ns after the fall of the short pulses.

* csontos@dept.phy.bme.hu

- [1] *International Technology Roadmap for Semiconductors* (2012), URL <http://www.itrs.net/>.
- [2] R. Chau, B. Doyle, S. Datta, J. Kavalieros, and K. Zhang, *Nat. Mater.* **6**, 810 (2007).
- [3] K. Kuhn, *IEEE Trans. Electron Devices* **59**, 1813 (2012).
- [4] J. R. Heath and M. A. Ratner, *Physics Today* **56**, 43 (2003).
- [5] C. Schirm, M. Matt, F. Pauly, J. C. Cuevas, P. Nielaba, and E. Scheer, *Nat. Nano* **8**, 645 (2013).
- [6] J. J. Yang, D. B. Strukov, and D. R. Stewart, *Nat. Nano* **8**, 13 (2013).
- [7] K. Terabe, T. Hasegawa, T. Nakayama, and M. Aono, *Nature* **433**, 47 (2005).
- [8] D. B. Strukov, G. S. Snider, D. R. Stewart, and R. S. Williams, *Nature* **453**, 80 (2008).

[9] R. Waser and M. Aono, *Nat. Mater.* **6**, 833 (2007).

[10] K. Terabe, T. Hasegawa, C. Liang, and M. Aono, *Adv. Mater.* **8**, 536 (2007).

[11] M. Aono and T. Hasegawa, *IEEE Proc.* **898**, 2228 (2010).

[12] E. Linn, R. Rosezin, C. Kugeler, and R. Waser, *Nat. Mater.* **9**, 403 (2010).

[13] A. C. Torrezan, J. P. Strachan, G. Medeiros-Ribeiro, and R. S. Williams, *Nanotechnology* **22**, 485203 (2011).

[14] R. Waser, R. Dittmann, G. Staikov, and K. Szot, *Adv. Mater.* **21**, 2632 (2009).

[15] L. Chua, *IEEE Trans. Circuit Theory* **18**, 507 (1971).

[16] Y. V. Pershin and M. Di Ventra, *Adv. Phys.* **60**, 145 (2011).

[17] K. Terabe, T. Nakayama, T. Hasegawa, and M. Aono, *J. Appl. Phys.* **91**, 10110 (2002).

[18] M. Morales-Masis, S. J. van der Molen, W. T. Fu, M. B. Hesselberth, and J. M. van Ruitenbeek, *Nanotechnology* **20**, 095710 (2009).

[19] M. Morales-Masis, H.-D. Wiemhöfer, and J. M. van Ruitenbeek, *Nanoscale* **2**, 2275 (2010).

[20] M. Morales-Masis, S. J. van der Molen, T. Hasegawa, and J. M. van Ruitenbeek, *Phys. Rev. B* **84**, 115310 (2011).

[21] A. Geresdi, A. Halbritter, A. Gyenis, P. Makk, and G. Mihály, *Nanoscale* **3**, 1504 (2011).

[22] Z. Xu, Y. Bando, W. Wang, X. Bai, and D. Golberg, *ACS Nano* **4**, 2515 (2010).

[23] Z. Wang, T. Kadohira, T. Tada, and S. Watanabe, *Nano Lett.* **7**, 2688 (2007).

[24] Z. Wang, T. Gu, T. Tada, and S. Watanabe, *Appl. Phys. Lett.* **93**, 152106 (2008).

[25] J. J. T. Wagenaar, M. Morales-Masis, and J. M. van Ruitenbeek, *J. Appl. Phys.* **111**, 014302 (2012).

[26] T. Hasegawa, T. Ohno, K. Terabe, T. Tsuruoka, T. Nakayama, J. K. Gimzewski, and M. Aono, *Adv. Mater.* **22**, 1831 (2010).

[27] T. Ohno, T. Hasegawa, T. Tsuruoka, K. Terabe, J. K. Gimzewski, and M. Aono, *Nat. Mater.* **10**, 591 (2011).

[28] M. D. Pickett, G. Medeiros-Ribeiro, and R. S. Williams, *Nat. Mater.* **12**, 114 (2013).

[29] A. Nayak, T. Tamura, T. Tsuruoka, K. Terabe, S. Hosaka, T. Hasegawa, and M. Aono, *J. Phys. Chem. Lett.* **1**, 604 (2010).

[30] A. Geresdi, A. Halbritter, E. Szilágyi, and G. Mihály, *MRS Proceedings* **1331** (2011).

[31] A. F. Andreev, *Sov. Phys. JETP* **19**, 1228 (1964).

[32] G. E. Blonder, M. Tinkham, and T. M. Klapwijk, *Phys. Rev. B* **25**, 4515 (1982).

[33] J. C. Cuevas, A. Martín-Rodero, and A. Levy Yeyati, *Phys. Rev. B* **54**, 7366 (1996).

[34] R. J. Soulen, J. M. Biers, M. S. Ofosky, B. Nadgorny, T. Ambrose, S. F. Cheng, P. R. Broussard, C. T. Tanaka, J. Nowak, J. S. Moodera, et al., *Science* **282**, 85 (1998).

[35] E. Kótai, *Nucl. Instrum. Methods B* **85**, 588 (1994).

[36] R. Landauer, *Philos. Mag.* **21**, 863 (1970).

[37] Y. V. Nazarov and Y. M. Blanter, *Quantum Transport: Introduction to Nanoscience* (Cambridge University Press, 2009).

[38] A. Pleceník, M. Grajcar, Š. Beňačka, P. Seidel, and A. Pfuch, *Phys. Rev. B* **49**, 10016 (1994).

[39] A. Geresdi, A. Halbritter, M. Csontos, S. Csonka, G. Mihály, T. Wojtowicz, X. Liu, B. Jankó, and J. K. Furdyna, *Phys. Rev. B* **77**, 233304 (2008).

[40] J. Zemek, P. Jiricek, S. Hucek, A. Jablonski, and B. Lesiak, *Surf. Sci.* **473**, 8 (2001).

[41] J. Williams, *Linear Technology Application Note*, vol. 47 (1991), URL <http://cds.linear.com>.